Solid S ences 12 (2010) 1160–1

Contents lists available at ScienceDirect

Solid State Sciences

journal homepage: www.elsevier.com/locate/ssscie

Structure and optical properties of $[Ba_{}Y_{2x/3}](Zr_{0.25}Ti_{0.75})O_3$ powders

J.C. Sczancoski [a], L.S. Cavalcante [b,*], T. Badapanda [c], S.K. Rout [d], S. Panigrahi [c], V.R. Mastelaro [e], J.A. Varela [b], M. Siu Li [e], E. Longo [b]

[a] Universidade Federal de São Carlos, P.O. Box 676, 13565 905, São Carlos, SP, Brazil
[b] Universidade Estadual Paulista, P.O. Box 355, 14801 907, Araraquara, SP, Brazil
[c] Department of Physics, National Institute of Technology, Rourkela 769008, India
[d] Department of Applied Physics, Birla Institute of Technology, Mesra, Ranchi 835215, India
[e] IFSC, Universidade de São Paulo, P.O. Box 369, 13560 970, São Carlos, SP, Brazil

ARTICLE INFO

Article history:
Received 10 December 2009
Received in revised form
19 March 2010
Accepted 6 April 2010
Available online 10 April 2010

Keywords:
$Ba(Zr,Ti)O_3$
Vacancies
Lattice defects
Band gap
Photoluminescence

ABSTRACT

$[Ba_{1-x}Y_{2x/3}](Zr_{0.25}Ti_{0.75})O_3$ powders with different yttrium concentrations ($x = 0$, 0.025 and 0.05) were prepared by solid state reaction. These powders were analyzed by X-ray diffraction (XRD), Fourier transform Raman scattering (FT-RS), Fourier transform infrared (FT-IR) and X-ray absorption near-edge (XANES) spectroscopies. The optical properties were investigated by means of ultraviolet–visible (UV–vis) absorption spectroscopy and photoluminescence (PL) measurements. Even with the addition of yttrium, the XRD patterns revealed that all powders crystallize in a perovskite-type cubic structure. FT-RS and FT-IR spectra indicated that the presence of $[YO_6]$ clusters is able to change the interaction forces between the O–Ti–O and O–Zr–O bonds. XANES spectra were used to obtain information on the off-center Ti displacements or distortion effects on the $[TiO_6]$ clusters. The different optical band gap values estimated from UV–vis spect gested the existence of intermediary energy levels (shallow or deep holes) within the band gap. PL measurements carried out with a 350 nm wavelength at room temperature showed that all powders present typical broad band emissions in the blue region.

1. Introduction

In the last years, the lead-free ceramic oxides have been widely studied due to its dielectric, ferroelectric, electromechanical and piezoelect operties [1–6]. Besides the high thermal stability, these materials do not present detrimental effects to human health and/or environment [7–9]. Currently, considering the compounds belong to the perovskite-type group, the barium strontium titanate $(Ba,Sr)TiO_3$ (BST) has been considered a promising material for the development of tunable microwave devices because of its strong electric field dependence of dielectric constant. In spite of this interesting electrical property, the main drawback is related to its considerable dielectric loss at high frequencies [10–13]. The barium zirconate titanate $Ba(Zr_xTi_{1-x})O_3$ (BZT) has received more attention in the field of materials science by reason of its structural and physical properties exhibit a significant dependency with the titanium (Ti) and zirconium (Zr) contents into the matrix [14,15]. In fact, the researches with this perovskite [16–18] have been mainly focused on the dielectric properties as well as on the phase transition from ferroelectric to relaxor. In this case, in order to improve the electrical properties, the BZT ceramics have been doped with different lanthanides, semi-metal and alkaline-earth metals, such as: niobium [19], boron [20,21], lithium [17], yttrium [22], copper [23], vanadium [24], tungsten [25], manganese [26], nickel [27], aluminium [28], bismuth [23,29], lanthanum [30], cerium [31], samarium–europium–dysprosium [32], erbium [33] and ytterbium [34].

However, there are few studies reported in the literature on the optical properties of this compound. For example, Liu et al. [35] analyzed the infrared optical properties of BZT thin films prepared by the sol–gel method, using only two Zr concentrations ($x = 0.20$ and 0.30) into the lattice. They observed that the refractive indexes (n) of these thin films are lower when compared with those of $BaTiO_3$ single crystals in the wavelength range from 2500 to 12 000 nm. In terms of photoluminescence (PL) measurements at room temperature, the BZT phase (thin films or powders) has shown typical blue and orange emissions. In general, the origin of the PL phenomenon has been attributed to the degree of structural order–disorder into the lattice, as a consequence of the symmetry break between the O–Zr–O and O–Ti–O bonds [36–39].

Therefore, in this work, we report on the structure and optical properties of $[Ba_{1-x}Y_{2x/3}](Zr_{0.25}Ti_{0.75})O_3$ powders synthesized with

* Corresponding author. Tel.: +55 16 3361 5215, +55 16 8812 7437 (mobile).
E-mail address: laeciosc@bol.com.br (L.S. Cavalcante).

1293-2558/$ – see front matter © 2010 Elsevier Masson SAS. All rights reserved.
doi:10.1016/j.solidstatesciences.2010.04.002

different yttrium (Y) concentrations ($x = 0$, 0.025 and 0.05) by the solid state reaction method.

2. Experimental procedure

2.1. Synthesis and characterizations of $[Ba_{1-x}Y_{2x/3}](Zr_{0.25}Ti_{0.75})O_3$ powders obtained by solid state reaction

$[Ba_{1-x}Y_{2x/3}](Zr_{0.25}Ti_{0.75})O_3$ powders were prepared by solid state reaction route [40]. In this synthesis method, barium carbonate ($BaCO_3$) (99%, Fine Chem., Mumbai), titanium oxide (TiO_2) (99.9%, E. Merck India Ltd.), zirconium oxide (ZrO_2) (99.9%, Loba Chem., Mumbai) and yttrium oxide (Y_2O_3) (99.9% E. Merck India Ltd) were used as raw materials. These compounds were stoichiometrically mixed using isopropyl alcohol (IPA) and milled with an agate mortar up to obtain homogenous powders. Afterwards, these powders were heat treated successively at 1350 °C for 6 h in a conventional furnace.

The synthesized powders were structurally characterized by XRD using a DMax/2500 PC diffractometer (Rigaku, Japan). The XRD patterns were obtained with Cu Kα radiation in the 2θ range from 10° to 75°, using a scanning rate of 0.2°/s. The FT-RS measurements were carried out with an RFS/100 spectrophotometer (Bruker, Germany). In this equipment, a Nd:YAG ion laser ($\lambda = 1064$ nm) was used to obtain the FT-RS spectra, keeping its maximum output power at 105 mW. The FT-IR spectra were obtained by means of an Equinox 55 (Bruker, Germany) spectrophotometer, using a 30° specular reflectance accessory. The XANES spectra were performed at the LNLS (National Synchrotron Light Laboratory-Brazil), using the D04B-XAS1 beam line. The LNLS storage ring was operated at 1.36 GeV with an electron beam current in the range from 180 to 250 mA. The XANES data were collected at the Ti K-edge (4966 eV) in transmission mode with a channel-cut Si(111) monochromator. These spectra were recorded from 4910 to 5100 eV, using energy steps of 0.3 eV around the edge. The monochromator energy calibration was checked during the XANES data collection through a titanium (Ti) metal foil. The UV–vis spectra were taken with a Cary 5G (Varian, USA) spectrophotometer in diffuse reflection mode. The PL measurements were performed through a Monospec 27 monochromator (Thermal Jarrel Ash, USA) coupled to an R446 photomultiplier (Hamamatsu, Japan). A krypton ion laser (Coherent Innova 90 K, USA) ($\lambda = 350$ nm) was employed as excitation source, keeping its maximum output power at 200 mW. The UV–vis and PL spectra were taken three times for each sample in order to ensure the reliability of the results. All measurements were performed at room temperature.

3. Results and discussion

3.1. X-ray diffraction analyses

Fig. 1(a) shows the XRD patterns of $[Ba_{1-x}Y_{2x/3}](Zr_{0.25}Ti_{0.75})O_3$ powders ($x = 0$, 0.025 and 0.05). The lattice parameters and the unit cell volumes for all powders were calculated through the UNITCELL-97 program [41], using the regression diagnostics combined with nonlinear least squares as illustrated in Fig. 1(b).

In Fig. 1(a), the XRD patterns indicated that all powders crystallize in a perovskite-type cubic structure with space group $Pm\bar{3}m$, in agreement with the respective Joint Committee on Powder Diffraction Standards (JCPDS) card No. 36-0019 [42]. Diffraction peaks related to the Y_2O_3 (secondary phase) were not detected, suggesting that the Y atoms were incorporated into the $[Ba_{1-x}Y_{2x/3}](Zr_{0.25}Ti_{0.75})O_3$ structure. However, it was noted that the increase of Y_2O_3 content into the host matrix promoted a slight reduction in the lattice parameter values as well as a contraction of the unit cell

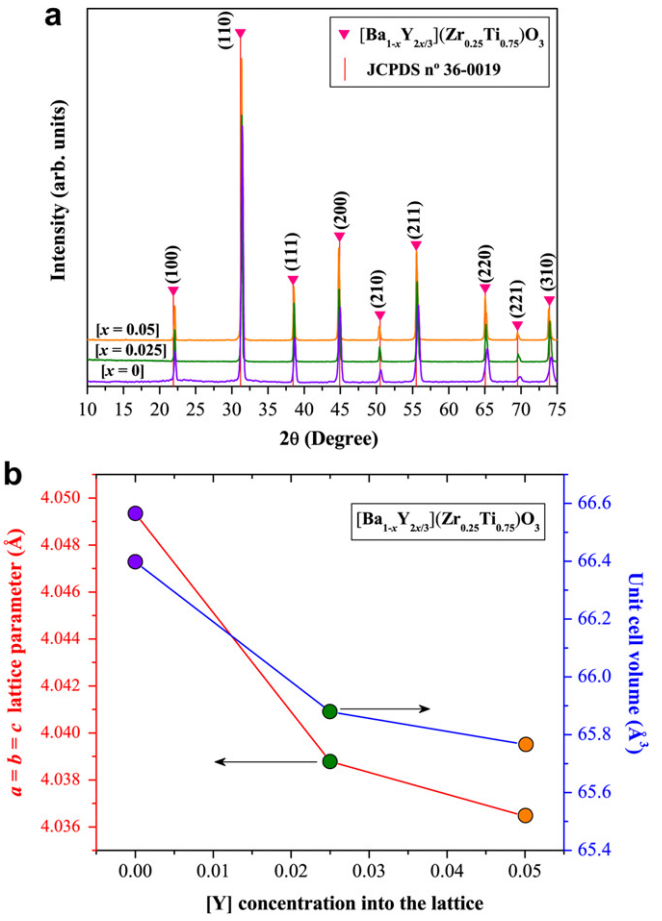

Fig. 1. (a) XRD patterns and (b) lattice parameter values as well as unit cell volume of $[Ba_{1-x}Y_{2x/3}](Zr_{0.25}Ti_{0.75})O_3$ ($x = 0$, 0.025 and 0.05).

volume (Fig. 1(b)). According to Shan et al. [43], the substitution of Ba sites by Y leads to the distortions into the BZT structure because of the different atomic radii. The literature reports that the ionic radius of Ba^{2+} ions is approximately 0.161 nm, while those of Y^{3+} is 0.086 nm [44–46]. Based on these hypotheses, we suppose that the substitution of Ba sites commonly occupied by Y atoms causes an electronic compensation through the formation of barium vacancies (V_{Ba}^{x}, V_{Ba}' or V_{Ba}''). In this case, it is very probable that the Y atoms are coordinated to six oxygen (O) atoms (distorted $[YO_6]$ clusters), while the Ba atoms are bonded to twelve oxygen atoms ($[BaO_{12}]$ clusters) [40]. Hence, the substitution processes of $[BaO_{12}]$ by distorted $[YO_6]$ clusters can be described by the following Kröger–Vink equation [46]:

$$Y_2O_3 \rightarrow 2Y_{Ba}^{\bullet} + V_{Ba}'' + 3O_O^x \quad (1)$$

In principle, this equation suggests that the increase of $[YO_6]^{\bullet}$ clusters into the $[Ba_{1-x}Y_{2x/3}](Zr_{0.25}Ti_{0.75})O_3$ structure promotes to formation of $V_{Ba}''^{\bullet}$

3.2. Superstructures with distorted clusters for the $[Ba_{1-x}Y_{2x/3}](Zr_{0.25}Ti_{0.75})O_3$ lattices

Fig. 2 shows the schematic representation of crystalline $[Ba_{1-x}Y_{2x/3}](Zr_{0.25}Ti_{0.75})O_3$ supercells ($1 \times 2 \times 2$) with two different Y concentrations: (a) $x = 0$ and (b) $x = 0.025$ or 0.05.

In these supercells, both Ti and Zr atoms (lattice formers) are bonded to six O atoms, forming the $[TiO_6]$ and $[ZrO_6]$ clusters (Fig. 2 (a, b)). However, there is a distinct difference between these two

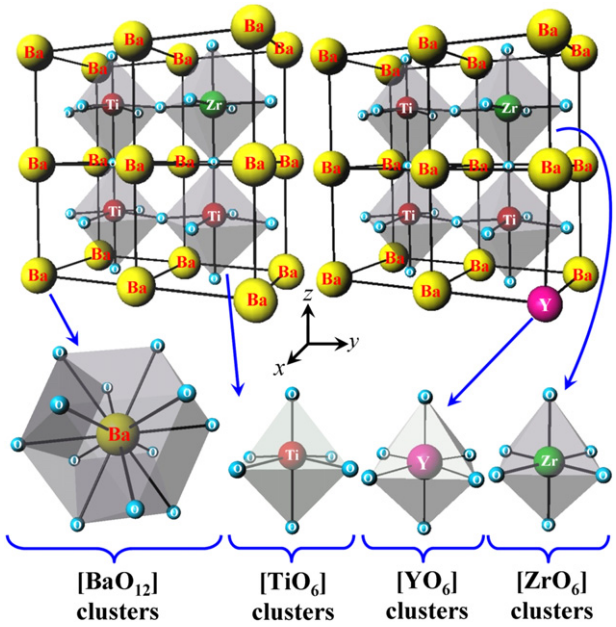

Fig. 2. Schematic representation of crystalline $[Ba_{1-x}Y_{2x/3}](Zr_{0.25}Ti_{0.75})O_3$ supercells ($1 \times 2 \times 2$) for (a) $x = 0$ and (b) $x = 0.25$, illustrating the $[TiO_6]$, $[ZrO_6]$, $[YO_6]$ and $[BaO_{12}]$ clusters.

clusters. In the non-polar $[ZrO_6]$ clusters, the Zr atoms are located in a centrosymmetric position into the octahedron. On the other hand, in the polar $[TiO_6]$ clusters, the Ti atoms are slightly displaced along the [001] direction (*z*-axis) [47]. This displacement or distortion can be arising from the covalent character between the O–Ti–O bonds (directional orientations) [48,49]. Analyzing only the lattice modifiers, each Ba atom is bonded to the twelve O (radial orientations) in a dodecahedral configuration ($[BaO_{12}]$ clusters) (Fig. 2(a)). According to the literature [40] describes that the structural organization as well as the polarization mechanisms into the cubic BZT structure are related to the presence of polar $[TiO_6]$ clusters close to those of $[BaO_{12}]$. Fig. 2(b) shows a crystalline $[Ba_{1-x}Y_{2x/3}](Zr_{0.25}Ti_{0.75})O_3$ supercell, where the Y atoms are coordinated to the six O in an octahedral configuration ($[YO_6]$ clusters) [50].

3.3. Fourier transform Raman scattering spectroscopy analyses

Fig. 3 shows the FT-RS spectra of $[Ba_{1-x}Y_{2x/3}](Zr_{0.25}Ti_{0.75})O_3$ powders ($x = 0$, 0.025 and 0.05).

Although the $[Ba_{1-x}Y_{2x/3}](Zr_{0.25}Ti_{0.75})O_3$ powders ($x = 0$, 0.025 and 0.05) crystallize in a cubic phase, the FT-RS spectra indicated the presence of seven Raman-active modes. This fact can be due to the structural order–disorder induced by the successive milling cycles and/or because of the distortions caused by the substitution of $[BaO_{12}]$ clusters by those of $[YO_6]$. According to the literature [51,52], these Raman-active modes can be divided into longitudinal (LO) and transverse (TO) components, as a consequence of the long-range electrostatic forces responsible for the lattice ionicity.

A closer analysis of the FT-RS spectrum for the pure Ba $(Zr_{0.25}Ti_{0.75})O_3$ phase indicated the presence of $A_1(TO_1)$ and $A_1(TO_3)$ modes at around 180 cm^{-1} and 514 cm^{-1}, respectively. The $A_1(TO_1)$ mode is ascribed to the O–Ti–O symmetric stretching vibrations, while the $A_1(TO_3)$ mode is due to the asymmetric vibrations [53,54]. In addition, the $E(TO_1)$ and $E(TO_2)$ modes detected at around 114 cm^{-1} and 305 cm^{-1} correspond to the phase transition from tetragonal to cubic crystal structure [55]. Actually, for the Ba $(Zr_{0.25}Ti_{0.75})O_3$ phase, these modes indicate a high concentration of polar $[TiO_6]$ distorted clusters into a predominantly cubic matrix.

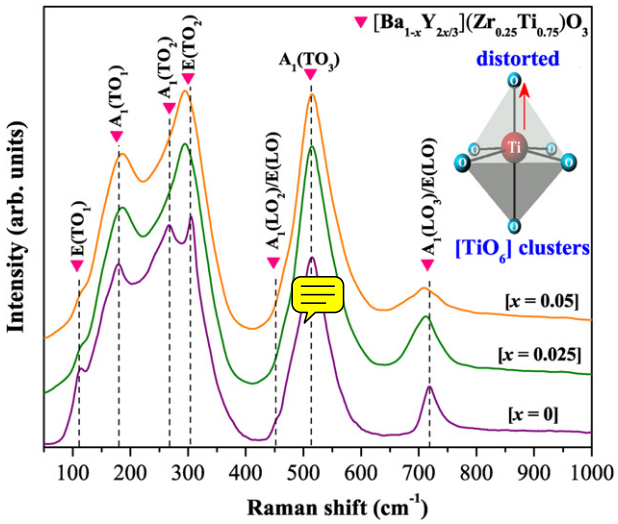

Fig. 3. FT-RS spectra of $[Ba_{1-x}Y_{2x/3}](Zr_{0.25}Ti_{0.75})O_3$ powders ($x = 0$, 0.025 and 0.05). The vertical dashed lines indicate the positions and relative intensities of Raman-active modes.

The $E(TO_2)$ stretching mode is particularly observed in FT-RS spectra because of the existence of polar $[TiO_6]$ clusters into the perovskite-type structure. Moreover, the intensity exhibited by this mode in the $Ba(Zr_{0.25}Ti_{0.75})O_3$ phase is lower when compared to the $BaTiO_3$ [56]. A plausible explanation for this phenomenon has been reasoned in the assumption that the distribution of non-polar $[ZrO_6]$ clusters into the lattice reduces the dipolar interactions between the polar $[TiO_6]$ clusters [57]. Also, these kinds of clusters are responsible for the $A_1(LO_3)$ mode observed at 718 cm^{-1} [40]. The other Raman-active modes detectable in the FT-RS spectra are arising from lattice vibrations along the LO and TO directions.

Also, when the Y atoms were incorporated into the Ba $(Zr_{0.25}Ti_{0.75})O_3$ structure, some Raman-active modes presented a subtle displacement [$A_1(TO_1)$, $E(TO_2)$, $A_1(LO_3)$ and $E(LO)$] or disappearance $A_1(TO_1)$ in the FT-RS spectra (Fig. 3). This observation can be correlated with the increase in the degree of symmetry of the cubic structure (O_h) and/or because of the contraction in the unit cell volume by the $[YO_6]$ clusters. In particular, the overlap between the $A_1(TO_2)$ and $E(TO_2)$ modes can be due to a reduction in the electronic density around the $[YO_6]$ clusters.

3.4. Fourier transform infrared spectroscopy analyses

Fig. 4 shows the FT-IR spectra of $[Ba_{1-x}Y_{2x/3}](Zr_{0.25}Ti_{0.75})O_3$ ($x = 0$, 0.025 and 0.05).

From the FT-IR spectra one get information about the role of $[YO_6]$ clusters in $Ba(Zr_{0.25}Ti_{0.75})O_3$ crystal lattice [58]. The pure Ba $(Zr_{0.25}Ti_{0.75})O_3$ crystal phase is characterized by the absorption band at 536 cm^{-1} due to anti-symmetric stretching vibrations of metal–oxygen bonds ($[TiO_6]$ and $[ZrO_6]$ clusters). The substitution of $[BaO_{12}]$ by $[YO_6]$ clusters creates not only V_{Ba}^{x}, V'_{Ba} or V_{Ba}'' vacancies but also internal stresses on the octahedral sites ($[TiO_6]$ and/or $[ZrO_6]$ clusters) [59,60]. The substitution process can then modify the interaction forces between the O–Ti–O and O–Zr–O bonds, what can lead to considerable displacement of the absorption band to high wave number region (568 cm^{-1} and 570 cm^{-1}).

3.5. X-ray absorption near-edge spectroscopy analyses

Fig. 5(a) shows the general Ti K-edge XANES spectra both $BaTiO_3$ and $[Ba_{1-x}Y_{2x/3}](Zr_{0.25}Ti_{0.75})O_3$ powders ($x = 0$, 0.025 and 0.05). In Fig. 5(b) is illustrated the pre-edge region situated in the range from

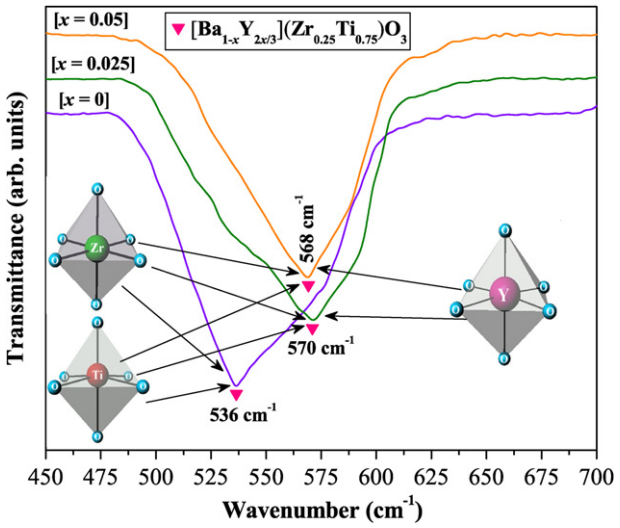

Fig. 4. FT-IR spectra of $[Ba_{1-x}Y_{2x/3}](Zr_{0.25}Ti_{0.75})O_3$ powders ($x = 0$, 0.025 and 0.05). The inset indicates the absorption bands corresponding to the $[TiO_6]$, $[ZrO_6]$ and $[YO_6]$ clusters.

4960 to 4976 eV. The calculated pre-edge peak areas for all powders as well as the off-center Ti displacements into the octahedral sites are shown in Fig. 5(c). The percentages of distorted $[TiO_6]$ clusters into these perovskites are displayed in Fig. 5(d).

The XANES technique became a powerful tool in the description of electronic structures of amorphous and crystalline compounds [61]. Moreover, the XANES spectra are very efficient to obtain information on the structural order at short-range of the materials, such as: coordination environment (tetrahedral, octahedral, dodecahedral,…), oxidation state and subtle lattice distortions [62]. In Fig. 5(a), it was detected a small peak located at around 4970 eV (•) known as pre-edge region, which corresponds to the $1s \rightarrow 3d$ electronic transitions [62,63]. Normally, there is a probability of this forbidden electronic transition to be allowed because of a mixture between the occupied O $2p$ orbitals and empty Ti $3d$ orbitals [64]. The intensity variations of the pre-edge peaks (•) are caused by the degree of hybridization associated to the O $2p$ and Ti $3d$ states of the $[TiO_6]$ clusters (Inset Fig. 5(a)). The literature [65] explains that the local Ti displacement (noncentrosymmetric) into the $[TiO_6]$ clusters leads to progressive increase in the pre-edge peak intensities. In fact, Farges et al. [66] reported that the energy and intensity associated to this peak for the titanate-based perovskite oxides can be classified into three distinct groups, depending on the coordination number of Ti–O bonds (four, five and six). As it can be seen in Fig. 5 (b), practically there are not modifications on the relative positions of the pre-edge peaks, suggesting only the existence of hexacoordinated Ti atoms ($[TiO_6]$ clusters). In order to qualitatively estimate the displacement presented by the Ti atoms into the $[TiO_6]$ clusters, it was employed the method proposed by Frenkel et al. [67]. According to these authors, the pre-edge peak area (A) in perovskite-type titanates is proportional to the square of the off-center Ti displacement (d_{Ti}), which is described by the following equation:

$$A = \frac{\gamma_i}{3} d_{Ti}^2, \tag{2}$$

where γ_i is a constant ($BaTiO_3 = 11.2$ eV/Å) [68].

Based on this equation, the area of each pre-edge peak (•) was estimated (from 4967 eV to 4972.2 eV) by means of integration. In the calculus, the XANES spectrum of $BaTiO_3$ phase was adopted as reference for those of $[Ba_{1-x}Y_{2x/3}](Zr_{0.25}Ti_{0.75})O_3$ ($x = 0$, 0.025 and 0.05), since the distortion of Ti atoms along the [001] direction is well-known for this material in the literature [37,69,70]. On the other hand, mechanical calculations based on the density functional theory (DFT) [71] showed that all four phases (cubic, tetragonal, orthorhombic and rhombohedral) of $BaTiO_3$ ferroelectrics have local Ti distortions toward [111] (octahedral face).

In our case, taking into consideration just the lattice modifiers, the $BaTiO_3$ phase was assumed to present 100% $[TiO_6]$ clusters. However, the $[Ba_{1-x}Y_{2x/3}](Zr_{0.25}Ti_{0.75})O_3$ ($x = 0$, 0.025 and 0.05) is not composed only of $[TiO_6]$ clusters, but also by those of $[ZrO_6]$. Hence, the calculated pre-edge peak area for all compositions in this structure was subtracted from 25% (equivalent to the quantity of $[ZrO_6]$ clusters). These area data were used in Eq. (2) in order to estimate the off-center Ti displacements (d_{Ti}). The d_{Ti} results and its respective supercells with the off-center Ti sites along the [001] direction are shown in Fig. 5(c) and (d), respectively. Thus, it was obtained the following d_{Ti} values: $d_{Ti}(BaTiO_3) = 0.37$ Å $> d_{Ti} = 0.27$ Å $> d_{Ti} = 0.26$ Å $> d_{Ti} = 0.25$ Å. In principle, the low d_{Ti} value suggests that the addition of Zr atoms into the $BaTiO_3$ matrix reduces the structural disorder (Fig. 5). Also, it was noted that the Y concentration does not strongly influenced in the distortion of Ti sites. In the literature, some studies have been reported on the structural modifications caused by the concentration of Y^{3+} ions into the perovskite-based materials. For example, Potrepka et al. [72] and Shanthakumar et al. [73] showed through XANES measurements that the addition of Y^{3+} ions into the $(Ba_{0.60}Sr_{0.40})TiO_3$ lattice does not affect the average Ti displacement from the octahedron center. Besides these works, our results are in agreement with others reported in the literature [74,75].

3.6. Ultraviolet–visible absorption spectroscopy analyses

Fig. 6(a–c) shows the UV–vis absorption spectra of $[Ba_{1-x}Y_{2x/3}](Zr_{0.25}Ti_{0.25})O_3$ powders ($x = 0$, 0.025 and 0.05).

The optical band gap energy (E_{gap}) was estimated by the method proposed by Wood and Tauc [76]. According to these authors the optical band gap is associated with the absorbance and photon energy by the following equation:

$$h\nu\alpha \propto (h\nu - E_{gap})^n \tag{3}$$

where α is the absorbance, h is the Planck constant, ν is the frequency, E_{gap} is the optical band gap and n is a constant associated to the different types of electronic transitions ($n = 0.5$, 2, 1.5 or 3 for direct allowed, indirect allowed, direct forbidden and indirect forbidden transitions, respectively). Thus, the E_{gap} value of $[Ba_{1-x}Y_{2x/3}](Zr_{0.25}Ti_{0.25})O_3$ powders was evaluated extrapolating the linear portion of the curve or tail. In our work, the UV–vis absorbance spectra indicated an indirect allowed transition and, therefore, the value of $n = 2$ was used in Eq. (3). The literature [77] describes that the band gap energy is indirect when the electronic transitions occur from maximum-energy states located near or in the valence band (VB) to minimum-energy states below or in the conduction band (CB), but in different regions in the Brillouin zone.

The distinct E_{gap} calculated from the UV–vis absorption spectra indicated the existence of intermediary energy levels within the optical band gap (Fig. 6(a–c)). We believe in these results, since the excitation energy ($\lambda = 350$ nm or 3.54 eV) is higher than the E_{gap} presented for all powders. The highest E_{gap} value was verified for the powders with Y content up to $x = 0.025$, suggesting a different conformation or low concentration of energy states within the band gap. It is possible to conclude that these energy states are basically composed of O $2p$ orbitals (near the VB) as well as Ti $3d$ orbitals, Y and Zr $4d$ orbitals (below the CB) [78]. The origin of these

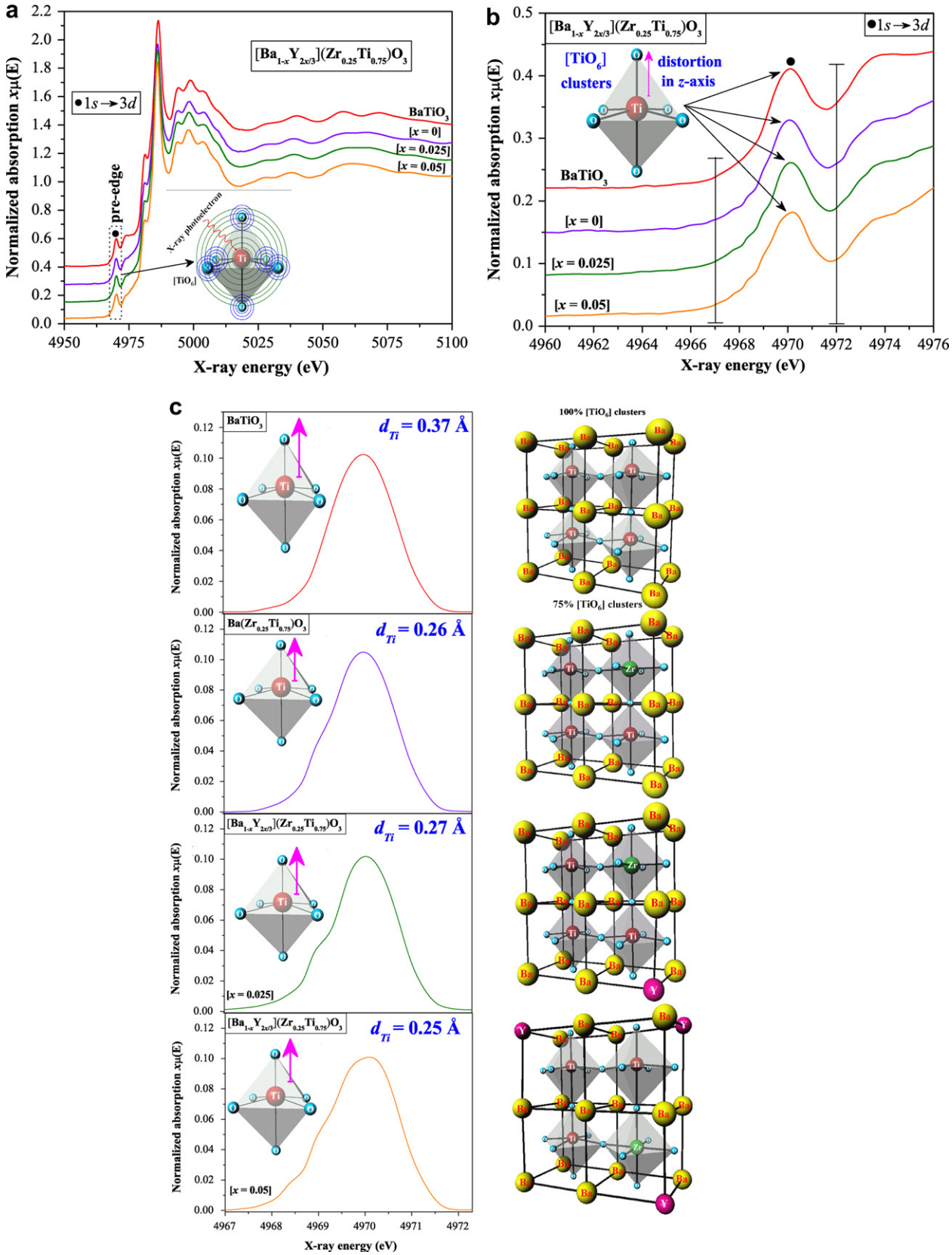

Fig. 5. (a) XANES spectra of $BaTiO_3$ and $[Ba_{1-x}Y_{2x/3}](Zr_{0.25}Ti_{0.75})O_3$ powders ($x = 0$, 0.025 and 0.05). The inset illustrates the X-ray photoelectron scattering, where the photoelectron excited at the atomic absorption site (Ti atoms) is scattered by the neighbor O atoms. (b) Pre-edge peak located in the range from 4960 to 4976 eV. The vertical lines indicate the positions where it was performed the baseline in order to calculate the pre-edge peak area. (c) The calculated pre-edge area. The insets illustrate the off-center Ti displacement for the octahedral sites. (d) Percentages of distorted $[TiO_6]$ clusters.

orbitals or energy levels is directly related to the presence of structural order–disorder into the random lattice, as a consequence of symmetry break between the O–Zr–O, O–Ti–O and/or O–Y–O bonds (oxygen vacancies) and/or distortions on the [TiO_6] clusters [79].

3.7. Photoluminescence properties and wide band model based on the electronic transitions

Fig. 7(a) shows the PL spectra of $[Ba_{1-x}Y_{2x/3}](Zr_{0.25}Ti_{0.75})O_3$ powders synthesized with different Y concentrations ($x = 0$, 0.025 and 0.05). A model based on electronic transitions between different intermediary energy levels within the band gap is illustrated in Fig. 7(b).

The broad PL spectra are optical phenomena caused by diverse electronic transitions occurring in different energy levels (deep or shallow holes) within the band gap [80]. The literature [39] reports that the deep holes are origin states for the green, yellow, orange and red PL emissions at room temperature, while the shallow holes are responsible for the violet and blue emissions. In our case, using an excitation source of 350 nm wavelength, the pure Ba$(Zr_{0.25}Ti_{0.75})O_3$ phase exhibited a weak PL emission, where the maximum point was detected at around 467 nm (blue emission) (Fig. 7(a)). Therefore, it is an indicative that the charge transference process as well as the trapping of electrons occurs because of a greater contribution of the shallow holes than the deep holes. In addition, for the $[Ba_{1-x}Y_{2x/3}](Zr_{0.25}Ti_{0.75})O_3$ powders ($x = 0.025$ and 0.05), the PL spectra revealed a slightly displacement from 467 nm to 460 nm as well as an increase in the intensity. This result suggests that when the Y atoms occupied the Ba sites into the perovskite, it contributed to the reorganization and formation of new energy levels (Y 4*d* orbitals). Also, the existence of hexacoordinated Y atoms ([YO_6] clusters) is able to promote the creation of barium vacancies (V_{Ba}^{x}, V'_{Ba} or V_{Ba}'') into the host matrix. When compared both the Y-doped $Ba(Zr_{0.25}Ti_{0.75})O_3$ powders, the PL spectra indicated a low intensity for those with Y content up to $x = 0.05$. In this case, this composition certainly formed a high concentration of structural defects, mainly barium vacancies, actuating as extinction centers of PL emission. Insets in Fig. 7(a) illustrate two examples of charge transference processes via distorted [TiO_6] clusters for the pure and Y-doped Ba$(Zr_{0.25}Ti_{0.75})O_3$ phases.

As it was previously described in the text, the $[Ba_{1-x}Y_{2x/3}](Zr_{0.25}Ti_{0.75})O_3$ phase is probably formed by O 2*p* orbitals (near the VB) as well as Ti 3*d* orbitals, Y and Zr 4*d* orbitals (below the CB). Thus, it was proposed a wide band model based on the electronic transitions between these intermediary energy levels in order to explain the origin of the PL emissions for this system (Fig. 7(b)). In the first stage, also known as excitation process, the electrons situated in the O 2*p* orbitals absorb the photon energies ($h\nu$) arising from incident wavelength ($\lambda = 350$ nm or 3.54 eV). Afterward, the energetic electrons are promoted to Ti 3*d* and/or Zr/Y 4*d* orbitals (higher energy states). Finally, when the electrons fall back again to lower energy states via radiative decays, the energies arising from these electronic transitions are converted in photons ($h\nu'$). In this case, the several photons ($h\nu'$) originated during the multiple radiative electronic transitions are responsible by the PL emissions (Fig. 7(b)).

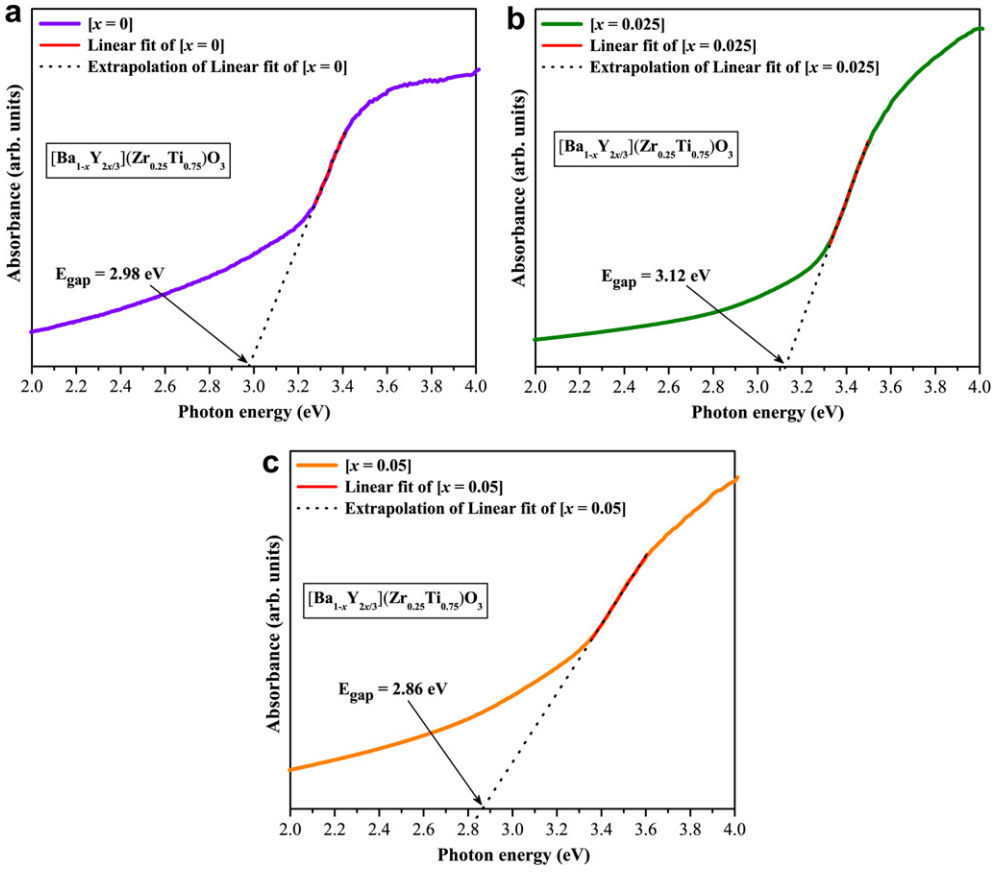

Fig. 6. UV–vis absorbance spectra of $[Ba_{1-x}Y_{2x/3}](Zr_{0.25}Ti_{0.75})O_3$ powders (x = (a) 0, (b) 0.025 and (c) 0.05).

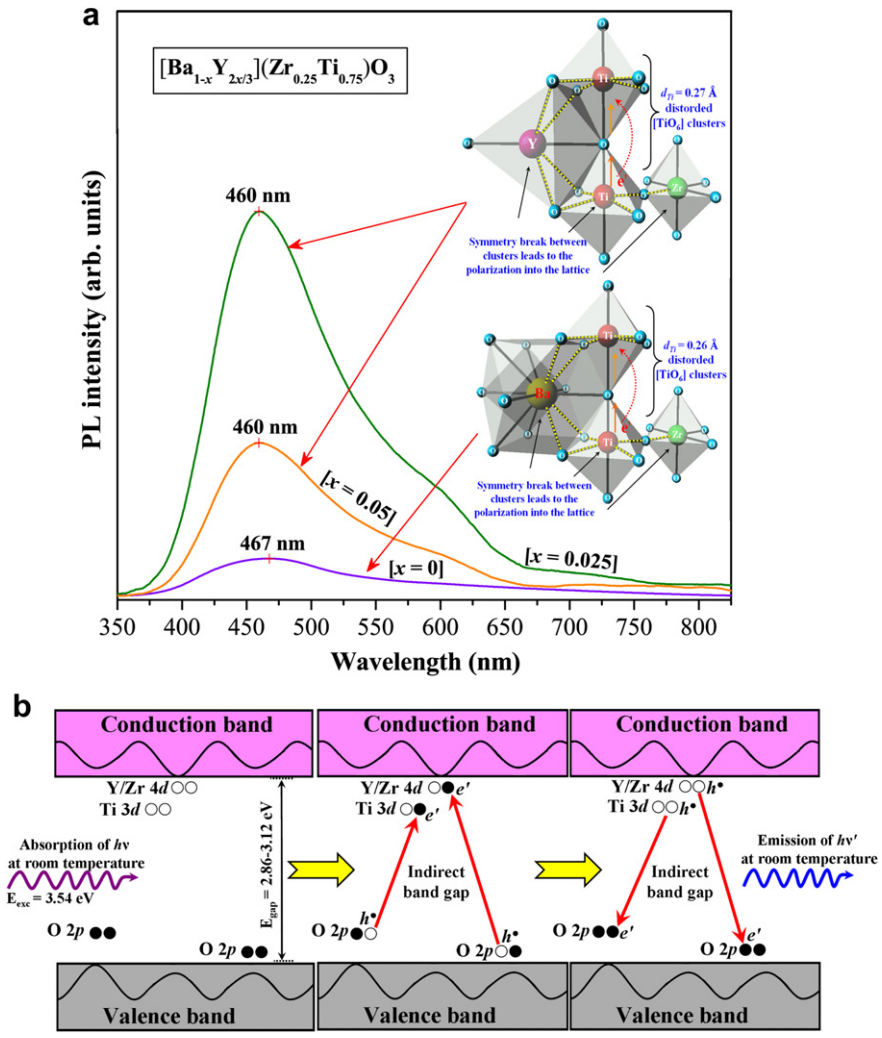

Fig. 7. (a) PL spectra at room temperature of $[Ba_{1-x}Y_{2x/3}](Zr_{0.25}Ti_{0.75})O_3$ powders ($x = 0$, 0.025 and 0.05). The insets show two possible charge transference processes between the distorted $[TiO_6]$ clusters. (b) Wide band model based on the electronic transitions between the O 2*p*, Ti 3*d*, Zr and Y 4*d* orbitals.

4. Conclusions

In summary, the $[Ba_{1-x}Y_{2x/3}](Zr_{0.25}Ti_{0.75})O_3$ powders with different Y concentrations ($x = 0$, 0.025 and 0.05) were prepared by solid state reaction under heat treatment conditions performed at 1350 °C for 6 h. XRD patterns showed that all powders have a cubic structure with space group $Pm\bar{3}m$. Secondary phases were not detected in the diffractograms, thus indicating that the Y atoms were incorporated into the $Ba(Zr_{0.25}Ti_{0.75})O_3$ matrix. Moreover, it was observed that the addition of Y leads to a slight contraction of the unit cell volume. In spite of the cubic structure, it was detected seven Raman-active modes in the FT-RS spectra, suggesting the occurrence of structural distortions on the polar $[TiO_6]$ clusters at short-range. Also, the displacement and disappearance of some Raman-active modes were associated to the structural modifications induced by the $[YO_6]$ clusters into the lattice. The displacement verified in the absorption band corresponding to the O–Ti–O and O–Zr–O bonds was correlated to the stresses induced on the $[TiO_6]$ and $[ZrO_6]$ clusters, as a consequence of the substitution of Ba atoms by those of Y. XANES spectra indicated that the Zr atoms minimize the structural disorder, while the Y atoms do not considerably contribute for the average Ti displacement into the polar $[TiO_6]$ clusters. UV–vis spectra suggested an indirect allowed transition with the existence of intermediary energy levels (shallow or deep holes) within the band gap. These energy states are formed of O 2*p*, Ti 3*d*, Zr and Y 4*d* orbitals. Finally, the origin of the blue PL emission was related to the several radiative electronic transitions between these different energy levels. In addition, the Y-doped Ba $(Zr_{0.25}Ti_{0.75})O_3$ powders exhibited a high PL intensity when compared to the pure $Ba(Zr_{0.25}Ti_{0.75})O_3$. This result was attributed the formation and reorganization of Y 4*d* orbitals within the band gap.

Acknowledgements

The authors thank the financial support of the Brazilian research financing institutions: FAPESP-Postdoctoral (N°. 2009/50303-4), CNPq, CAPES and LNLS (Projeto N°. D04B - XAFS1 - 8823).

References

[1] P. [illegible]a, K. Pengpat, P. Jarupoom, U. Intatha, G. Rujijanagul, T. Tunkasiri, Curr. Appl. Phys. 9 (2009) 460.
[2] C. Peng, J.F. Li, W. Gong, Mater. Lett. 59 (2005) 1576.
[3] D. Lin, K.W. Kwok, H.L.W. Chan, Mater. Chem. Phys. 109 (2008) 455.
[4] H. Maiwa, Jpn. J. Appl. Phys. 46 (2007) 7013.
[5] Z. Zhang, J. Jia, H. Yang, C. Chen, H. Sun, X. Hu, D. Yang, J. Mater. Sci. 43 (2008) 1501.
[6] Z. Chen, J. Hu, Ceram. Inter. 35 (2009) 111.

[7] M.Z.C. Hu, V. Kurian, E.A. Payzant, C.J. Rawn, R.D. Hunt, Powder Technol. 110 (2000) 2.
[8] Z. Chen, A. Shui, Z. Lu, P. Liu, J. Ceram. Soc. Japan 114 (2006) 857.
[9] T. Maiti, R. Guo, A.S. Bhalla, J. Am. Ceram. Soc. 91 (2008) 1769.
[10] J. Cui, G. Dong, Y. Wang, J. Du, J. Mater. Sci: Mater. Electron 20 (2009) 473.
[11] J. Zhang, J. Zhai, X. Chou, J. Shao, X. Lu, X. Yao, Act. Mater. 57 (2009) 4491.
[12] M. Makimoto, S. Yamashita, Microwave Resonators and Filters for Wireless. Springer, 2001, (Chapter 1), pp. 5.
[13] M.T. Sebastian, Dielectric Materials for Wireless Communication. Elsevier, 2008, (Chapter 3), pp. 58.
[14] H. Khemakhem, A. Simon, R. von der Mhll, J. Ravez, J. Phys.: Condens. Matter 12 (2000) 5951.
[15] A. Simon, J. Ravez, Solid State Sci. 5 (2004) 1459.
[16] T. Tsurumi, Y. Yamamoto, H. Kakemoto, S. Wada, H. Chazono, H. Kishi, J. Mater. Res. 17 (2002) 755.
[17] X. Chou, J. Zhai, J. Sun, X. Yao, Ceram. Intern. 34 (2008) 911.
[18] C. Fu, F. Pan, W. Cai, X. Deng, X. Liu, Mater. Scie. Poland 27 (2009) 891.
[19] W. Cao, J. Xiong, J. Sun, Mater. Chem. Phys. 106 (2007) 338.
[20] P. Jarupoom, K. Pengpat, S. Eitssayeam, G. Rujijanagul, AIP Conf. Proc. 1151 (2009) 25.
[21] P. Jarupoom, G. Rujijanagul, K. Pengpat, T. Tunkasiri, Adv. Mater. Res. 55–57 (2008) 149.
[22] T. Badapanda, S. Panigrahi, S.K. Rout, T.P. Sinha, S.I. Woo, J. Korean Phys. Soc. 55 (2009) 749.
[23] S. Mahajan, O.P. Thakur, D.K. Bhattacharya, K. Sreenivas, J. Phys. D: Appl. Phys. 42 (2009) 065413.
[24] F. Moura, A.Z. Simoes, L.S. Cavalcante, M.A. Zaghete, J.A. Varela, E. Longo, J. Alloys Compd. 466 (2008) L15.
[25] F. Moura, A.Z. Simões, L.S. Cavalcante, M. Zampieri, J.A. Varela, E. Longo, M. A. Zaghete, M.L. Simões, Appl. Phys. Lett. 92 (2008) 032905.
[26] W. Cai, C. Fu, J. Gao, X. Deng, J. Mater. Sci. Mater. Electron (2009). doi:10.1007/s10854-009-9913-4.
[27] W. Cai, J. Gao, C. Fu, L. Tang, J. Alloys Compd. 487 (2009) 668.
[28] W. Cai, C. Fu, J. Gao, X. Deng, J Mater Sci: Mater Electron (2009). doi:10.1007/s10854-009-9995-z.
[29] T. Badapanda, S.K. Rout, S. Panigrahi, T.P. Sinha, Curr. Appl. Phys. 9 (2009) 727.
[30] X. Chou, J. Zhai, X. Yao, Mater. Chem. Phys. 109 (2008) 125.
[31] X. Huang, C. Gao, X. Chen, H. Liu, G. Huang, X. Zheng, J. Rare Earths 22 (2004) 219.
[32] X. Chou, J. Zhai, H. Jiang, X. Yao, J. Appl. Phys. 102 (2007) 084106.
[33] E. Antonelli, M. Letonturier, J.C. M'Peko, A.C. Hernandes, J. Eur. Ceram. Soc. 29 (2009) 1449.
[34] A. Kerfah, K. Taibi, A. Guehria-Laidoudi, A. Simon, J. Ravez, Solid State Sci. 8 (2006) 613.
[35] A. Liu, J. Xue, X. Meng, J. Sun, Z. Huang, J. Chu, Appl. Surf. Sci. 254 (2008) 5660.
[36] L.S. Cavalcante, M. Anicete-Santos, J.C. Sczancoski, L.G.P. Simões, M.R.M. C. Santos, J.A. Varela, P.S. Pizani, E. Longo, J. Phys. Chem. Solids 69 (2008) 1782.
[37] L.S. Cavalcante, M.F.C. Gurgel, A.Z. Simões, E. Longo, J.A. Varela, M.R. Joya, P. S. Pizani, Appl. Phys. Lett. 90 (2007) 011901.
[38] S.K. Rout, L.S. Cavalcante, J.C. Sczancoski, T. Badapanda, S. Panigrahi, M. Siu Li, E. Longo, Physica B 404 (2009) 3341.
[39] L.S. Cavalcante, J.C. Sczancoski, F.S. De Vicente, M.T. Frabbro, M. Siu Li, J. A. Varela, E. Longo, J. Sol–Gel Sci. Technol. 49 (2009) 35.
[40] T. Badapanda, S.K. Rout, L.S. Cavalcante, J.C. Sczancoski, S. Panigrahi, E. Longo, M. Siu Li, J. Phys. D: Appl. Phys. 42 (2009) 175414.
[41] T.J.B. Holland, S.A.T. Redfern, Mineralogical Magazine 61 (1997) 65.
[42] Joint Committee on Powder Diffraction Standards, Diffraction Data File, No. 36–0019. International Centre for Diffraction Data (ICDD, formerly JCPDS), Newtown Square, PA, 2001.
[43] D. Shan, Y.F. Qu, J.J. Song, Solid State Commun. 141 (2007) 65.
[44] K. Watanabe, H. Ohsato, H. Kishi, Y. Okino, N. Kohzu, Y. Iguchi, T. Okuda, Solid State Ionics 108 (1998) 129.
[45] R.D. Shannon, Acta Crystallogr. A32 (1976) 751.
[46] F.A. Kröger, H.J. Vink, in: F. Seitz, D. Turnbull (Eds.), Solid State Physics, third ed. Academic Press, New York, 1956, p. 307.
[47] N. Jiang, D. Su, J.C.H. Spence, Phys. Rev. B 76 (2007) 214117.
[48] T. Maiti, E. Alberta, R. Guo, A.S. Bhalla, Mater. Lett. 60 (2006) 3861.
[49] T. Maiti, R. Guo, A.S. Bhalla, J. Appl. Phys. 100 (2006) 114109.
[50] C. Duan, J. Yuan, J. Zhao, J. Solid State Chem. 178 (2005) 3698.
[51] J.P. Crocombette, F. Jollet, J. Phys, Condens. Mater. 6 (1994) 8341.
[52] M.D. Domenico Jr., S.H. Wemple, S.P.S. Porto, P.R. Buman, Phys. Rev. 174 (1968) 522.
[53] A. Chaves, R.S. Katiyar, S.P.S. Porto, Phys. Rev. B 10 (1974) 3522.
[54] J. Kreisel, P. Bouvier, M. Maglione, S. Dkhil, A. Simon, Phys. Rev. B 69 (2004) 092104.
[55] P.S. Dobal, A. Dixit, R.S. Katiyar, Z. Yu, R. Guo, A.S. Bhalla, J. Appl. Phys. 89 (2001) 8085.
[56] B.D. Begg, K.S. Finnie, E.R. Vance, J. Am. Ceram. Soc. 79 (1996) 2666.
[57] A. Dixit, S.B. Majumder, P.S. Dobal, R.S. Katiyar, A.S. Bhalla, Thin Solid Films 447 (2004) 284.
[58] C. Ostos, L. Mestres, M.L. Martínez-Sarrión, J.E. Garca, A. Albareda, R. Perez, Solid State Sci. 11 (2009) 1016.
[59] D. Wang, R. Yu, S. Feng, W. Zheng, T. Takei, N. Kumada, N. Kinomura, Solid State Ionics 151 (2002) 329.
[60] N.K. Karan, R.S. Katiyar, T. Maiti, R. Guo, A.S. Bhalla, J. Raman Spectrosc. 40 (2008) 370.
[61] L.D. Menard, Q. Wang, J.H. Kang, A.J. Sealey, G.S. Girolami, X. Teng, Phys. Rev. B 80 (2009) 064111.
[62] S. de Lázaro, J. Milanez, A.T. de Figueiredo, V.M. Longo, V.R. Mastelaro, F.S. De Vicente, A.C. Hernandes, J.A. Varela, E. Longo, Appl. Phys. Lett. 90 (2007) 111904–111906.
[63] B. Ravel, C.E. Bouldin, H. Renevier, J.L. Hodeau, J.F. Berar, Phys. Rev. B 60 (1999) 778.
[64] R.V. Vedrinskii, V.L. Kraizman, A.A. Novakovich, P.V. Demekhin, S.V. Urazhdin, J. Phys.: Condens. Matter 10 (1998) 9561.
[65] A.I. Frenkel, Y. Feldman, V. Lyahovitskaya, E. Wachtel, I. Lubomirsky, Phys. Rev. B 71 (2005) 024116.
[66] F. Farges, G.E. Brown Jr., J.J. Rehr, Phys. Rev. B 56 (1997) 1809.
[67] A.I. Frenkel, D. Ehre, V. Lyahovitskaya, L. Kanner, E. Wachtel, I. Lubomirsky, Phys. Rev. Lett. 99 (2007) 215502–215505.
[68] B. Ravel, Ph.D. thesis, University of Washington, 1995.
[69] E. Orhan, J.A. Varela, A. Zenatti, M.F.C. Gurgel, F.M. Pontes, E.R. Leite, E. Longo, P.S. Pizani, A. Beltran, J. Andres, Phys. Rev. B 71 (2005) 085113.
[70] M.F.C. Gurgel, J.W.M. Espinosa, A.B. Campos, I.L.V. Rosa, M.R. Joya, A.G. Souza, M.A. Zaghete, P.S. Pizani, E.R. Leite, J.A. Varela, E. Longo, J. Lumin. 126 (2007) 771.
[71] Q. Zhang, T. Cagin, W.A. Goddard III, Proc. Natl. Acad. Sci. 103 (2006) 14695.
[72] D.M. Potrepka, S.C. Tidrow, A. Tauber, Integr. Ferroelectr 42 (2002) 97.
[73] P. Shanthakumar, M. Balasubramanian, D.M. Pease, A.I. Frenkel, D.M. Potrepka, V. Kraizman, J.I. Budnick, W.A. Hines, Phys. Rev. B 74 (2006) 174103.
[74] E.A.V. Ferri, J.C. Sczancoski, L.S. Cavalcante, E.C. Paris, J.W.M. Espinosa, A.T. de Figueiredo, P.S. Pizani, V.R. Mastelaro, J.A. Varela, E. Longo, Mater. Chem. Phys. 117 (2009) 192.
[75] N. Sicron, B. Ravel, Y. Yacoby, E.A. Stern, F. Dogan, J.J. Rehr, Phys. Rev. B 50 (1994) 13168.
[76] D.L. Wood, J. Tauc, Phys. Rev. B 5 (1972) 3144.
[77] L.S. Cavalcante, M.F.C. Gurgel, E.C. Paris, A.Z. Simões, M.R. Joya, J.A. Varela, P. S. Pizani, E. Longo, Acta Mater. 55 (2007) 6416.
[78] M. Anicete-Santos, L.S. Cavalcante, E. Orhan, E.C. Paris, L.G.P. Simões, M.R. Joya, I.L.V. Rosa, P.R. de Lucena, M.R.M.C. Santos, L.S. Santos-Júnior, P.S. Pizani, E. R. Leite, J.A. Varela, E. Longo, Chem. Phys. 316 (2005) 260.
[79] C. Laulhé, F. Hippert, R. Bellissent, A. Simon, G.J. Cuello, Phys. Rev. B 79 (2009) 064104.
[80] V.M. Longo, L.S. Cavalcante, R. Erlo, V.R. Mastelaro, A.T. de Figueiredo, J. R. Sambrano, S. de Lazaro, A.Z. Freitas, L. Gomes, N.D. Vieira, J.A. Varela, E. Longo, Acta Mater. 56 (2008) 2191.